# Formation of bubbly horizon in liquid-saturated porous medium by surface temperature oscillation

Denis S. Goldobin[1,2,3,*] and Pavel V. Krauzin[1]

[1]*Institute of Continuous Media Mechanics, UB RAS, 1 Academik Korolev str., Perm 614013, Russia*

[2]*Department of Theoretical Physics, Perm State University, 15 Bukireva str., Perm 614990, Russia*

[3]*Department of Mathematics, University of Leicester, University Road, Leicester LE1 7RH, United Kingdom*

(Received 12 October 2015; published 30 December 2015)

We study nonisothermal diffusion transport of a weakly soluble substance in a liquid-saturated porous medium in contact with a reservoir of this substance. The surface temperature of the porous medium half-space oscillates in time, which results in a decaying solubility wave propagating deep into the porous medium. In this system, zones of saturated solution and nondissolved phase coexist with ones of undersaturated solution. The effect is first considered for the case of annual oscillation of the surface temperature of water-saturated ground in contact with the atmosphere. We reveal the phenomenon of formation of a near-surface bubbly horizon due to temperature oscillation. An analytical theory of the phenomenon is developed. Further, the treatment is extended to the case of higher frequency oscillations and the case of weakly soluble solids and liquids.

DOI: 10.1103/PhysRevE.92.063032 PACS number(s): 47.55.db, 66.10.C−, 92.40.Kf

## I. INTRODUCTION

Diffusion transport in bubbly media [1–4] and media with a condensed nondissolved phase [2,5–7] appears to possess unique features under isothermal conditions and is even more intriguing under nonisothermal ones. For these systems, the nondissolved phase makes the local solute concentration equal to the solubility. The solute concentration is no longer a free variable, but a function of temperature and pressure. Simultaneously, the nonzero divergence of the solute flux determined by the solubility gradient does not change the enslaved solute concentration but redistributes the mass of the nondissolved phase. Thus, for the dynamics of systems with a nondissolved phase, novel phenomena and mechanisms, which never appear for undersaturated solutions, come into play. These phenomena are especially strongly pronounced for systems where the nondissolved phase is immobilized (e.g., in porous media) and solubility is low [3]. For an immobilized nondissolved phase, mass transport operates only through the solution, and when the solubility is low the mass accumulated in the nondissolved phase can be several orders of magnitude larger than the dissolved mass.

In Ref. [4], we reported the effect of surface temperature oscillations, which produce a solubility wave, on the diffusive transport in porous media where the nondissolved phase is present everywhere and discussed the physical systems for which the effect is relevant. Systems where zones with a nondissolved phase can coexist with zones of undersaturated solution can exhibit richer and more sophisticated dynamics. A liquid-saturated porous medium in contact with a reservoir of weakly soluble substance (e.g., atmosphere) is a system of this kind. In this paper we consider the effect of surface temperature oscillation on diffusive transport in the porous medium half-space in contact with a reservoir of a weakly soluble substance.

For the sake of definiteness, we consider transport of gases in detail and comment on how the results can be extended to the case of weakly soluble solids (e.g., limestone) and liquids (e.g., crude oil). The case of solids and liquids is different from the case of gases only in the insensitivity of the solubility to pressure. From the viewpoint of mathematics, for the processes under consideration, the case of gas hydrates is also identical to the case of weakly soluble solids.

Mathematically, the contact with the atmosphere is represented via the boundary condition; at the contact boundary the solute concentration equals the solubility at any instant in time. The same boundary condition and, consequently, the phenomena we report in this paper will hold for the case of contact with a reservoir of any substance.

In this paper, we reveal that the temperature wave leads to the formation of a near-surface bubbly horizon and "oversaturation" of the medium with the atmosphere gas compared to the period-mean solubility. In particular, the net molar fraction (nondissolved phase + solution) of the gas molecules in pores next to the surface equals the maximal-over-period solubility.

The phenomenon we report is common and can be important for various systems with different origins of the surface temperature oscillations, including technological systems (filters, porous bodies of nuclear and chemical reactors, etc.). However, for the sake of convenience, we first focus on the case characterized by the hydrostatic pressure gradient, which is significant for geological systems, where pressure doubles at the depth of 10 m, leading to a significant change in solubility. The no-pressure-gradient case is considered as well.

The effect of enhanced filling of water-saturated ground with atmospheric gases creates more favorable conditions for local microflora and fauna and influences conditions for geochemical processes. With weakly soluble solids, the effect provides opportunities for filling the porous matrix with some weakly soluble "guest" substance in technology; the spatial mass distribution pattern of the guest substance can be controlled by the surface temperature waveform. For natural methane hydrate deposits in seafloor sediments, the effect of temperature waves on the deposit and the gas release from it is of interest in relation to the natural glacial-interglacial cycles [8] and potential global climate change [9].

The paper is organized as follows. In Sec. II A, we introduce the physical model for diffusion transport of a weakly soluble substance in the presence of a nondissolved

*Denis.Goldobin@mail.ru

 

phase and governing equations. With the results of numerical simulation of governing equations for a single-gas-component atmosphere, we demonstrate the phenomenon of formation of a bubbly horizon in Sec. II B. The analytical theory of the phenomenon is developed in Sec. II C. In Sec. II D, we report the dependence of the integral quantifiers of the bubbly horizon on the control parameters of the system. In Sec. III, the case where the hydrostatic pressure gradient has no effect is studied (this case corresponds to high-frequency temperature oscillations or solutions of condensed phases). The results are summarized in Sec. IV, the Conclusion.

## II. DIFFUSION IN SATURATED AND UNDERSATURATED SOLUTIONS

### A. Physical model and governing equations

The diffusion transport of solute in the presence of a nondissolved phase is essentially controlled by the solubility. For moderate pressure and far from the solvent boiling point the solubility of gas in liquid reads [10]

$$X^{(0)}(T,P) \simeq X^{(0)}(T_0,P_0)\frac{T_0}{T}\frac{P}{P_0}\exp\left[q\left(\frac{1}{T}-\frac{1}{T_0}\right)\right], \quad (1)$$

where the molar solubility $X^{(0)}$ is the molar amount of solute per 1 mol of solvent, $T_0$ and $P_0$ are reference values, the choice of which is guided merely by convenience, and $X^{(0)}(T_0,P_0)$ is the solubility at the reference temperature and pressure; the parameter $q \equiv -G_i/k_B$, with $G_i$ being the interaction energy between a solute molecule and the surrounding solvent molecules and $k_B$ being the Boltzmann constant, is listed in Table I for several typical gases. For condensed matter (solids and liquids) the solubility is nearly independent of the pressure and approximately reads

$$X^{(0)}_{\rm cond}(T,P) \simeq X^{(0)}_{\rm cond}(T_0,P_0)\exp\left[q\left(\frac{1}{T}-\frac{1}{T_0}\right)\right]. \quad (2)$$

Geological systems are typically much more uniform in the horizontal directions than in the vertical one. Hence, it is reasonable to restrict our consideration to the one-dimensional case; the system is assumed to be homogeneous in the horizontal directions. We assume the $z$ axis to be oriented downwards and its origin to be on the porous medium surface.

Let us consider harmonic oscillation of the surface temperature, $T_0+\Theta_0\cos\omega t$, where $T_0$ is the mean temperature, $\Theta_0$ is the oscillation amplitude, and $\omega$ is the temperature oscillation cyclic frequency. In particular, annual oscillations of the surface temperature deviate only slightly from their harmonic reduction (e.g., see [11]). The heat diffusion equation $\partial T/\partial t = \chi\Delta T$ under no-heat-flux conditions deep below the surface (at infinity) and an imposed surface temperature yields

$$T(z,t) = T_0 + \Theta_0 e^{-kz}\cos(\omega t - kz), \quad k=\sqrt{\omega/2\chi}, \quad (3)$$

where $\chi$ is the heat diffusivity and $z$ is the distance from the surface of porous medium. The hydrostatic pressure field reads

$$P = P_0 + \rho g z, \quad (4)$$

where $P_0$ is the atmospheric pressure, $\rho$ is the liquid density, and $g$ is the gravity.

Since the nondissolved phase is immobilized in pores, the mass transport in the system is contributed solely by the diffusion through the intersticial liquid and governed by the equation

$$\frac{\partial X_\Sigma}{\partial t} = \nabla\cdot\left[DX_s\left(\frac{\nabla X_s}{X_s}+\alpha\frac{\nabla T}{T}\right)\right], \quad (5)$$

where $X_s$ is the molar concentration of the solution, $X_\Sigma = X_s + X_b$ is the net molar fraction of gas molecules in the interstitial fluid, $X_b$ is the molar fraction of the gaseous phase (bubbles) in the interstitial fluid, $D$ is the effective molecular diffusion coefficient, and $\alpha$ is the thermodiffusion constant [12]. Compared to the molecular diffusion coefficient in bulk of pure liquid, say $D_{\rm mol}$, the effective coefficient is influenced by the pore network geometry (tortuosity) and the adsorption of the diffusing agent on the porous matrix (on the time scales of our interest the adsorption does not lead to anomalous diffusion; it only changes the effective rate of normal diffusion [13]). The importance of thermal diffusion was demonstrated for gases [3] and methane hydrate [6,7] on geological time scales, although for the system of our interest it can be neglected [4]. Henceforth, we omit the thermal diffusion term. The solute concentration

$$X_s = \min\{X^{(0)}, X_\Sigma\}; \quad (6)$$

i.e., it equals the solubility $X^{(0)}$ where the net amount of gas molecules $X_\Sigma$ exceeds the solubility and equals $X_\Sigma$ otherwise. In the latter case, $X_b = 0$.

The formulated mathematical model of the system implies that the dissolution process (as well as the opposite process of formation of the nondissolved phase from the solution) occurs much more rapidly than the change in the temperature field and the diffusive redistribution of solute mass on macroscopic scales. In real systems, the dissolution time scales even for a solid nondissolved phase are assessed as hours (see [14]), which is short compared to the reference times of temperature oscillation and diffusive transport on the scale of the system. The hysteresis effects possible for some phase transformations in narrow pore channels [15] are neglected in our study.

Note that Eq. (5) is accurate for the case where the macroscopic porosity is spatially uniform and the nondissolved phase occupies a negligible fraction of the pore volume, which holds true for gases and weakly soluble solids and liquids. For the one-dimensional case, Eq. (5) takes the form

$$\frac{\partial X_\Sigma}{\partial t} = \frac{\partial}{\partial z}\left[D\frac{\partial X_s}{\partial z}\right]. \quad (7)$$

TABLE I. Chemical physical properties of solutions of nitrogen, oxygen, methane, and carbon dioxide in water. Equation (1), with $q$ and $X^{(0)}(T_0,P_0)$ specified in the table, fits the experimental data from [17]. Equation (10), with provided values of the effective radius $R_d$ and parameter $\nu$ of the solute molecules, fits the experimental data from [18].

| | $N_2$ | $O_2$ | $CH_4$ | $CO_2$ |
|---|---|---|---|---|
| $q=-G_i/k_B$ (K) | 781 | 831 | 1138 | 1850 |
| $X^{(0)}$ (20 °C, 1 atm) ($\times10^{-5}$) | 1.20 | 2.41 | 2.60 | 68.7 |
| $R_d$ ($10^{-10}$ m) | 1.48 | 1.29 | 1.91 | 1.57 |
| $\nu$ ($10^{-5}$ Pa · s) | 9.79 | 16.3 | 28.3 | 4.68 |

At the upper boundary we assume contact with the atmosphere, which means that

$$X_s(z=0,t) = X^{(0)}(T(z=0,t),P_0). \tag{8}$$

Deep below the surface we assume the no-flux condition and the absence of a nondissolved phase:

$$\left.\frac{\partial X_s}{\partial z}\right|_{z=+\infty} = 0, \quad X_b(z=+\infty) = 0. \tag{9}$$

Note that two boundary conditions are required at $z \to +\infty$; however, due to the specificity of our system, one boundary condition, Eq. (8), is sufficient at $z = 0$. Indeed, since $X_s(z=0)$ is never less than $X^{(0)}(z=0)$, the value of $X_b$ at the point $z = 0$ does not influence the system dynamics; the condition for it is redundant.

Generally, all material properties of the system depend on the temperature and pressure. However, feasible relative variations of the absolute temperature are small. Hence, one can neglect variation of those parameters which depend on the temperature polynomially and consider variation of only those parameters which depend on the temperature exponentially: the latter parameters are the solubility, (1), and the molecular diffusion coefficient $D$. Moreover, the only parameter sensitive to pressure is the gas solubility.

We employ the following dependence of molecular diffusion on temperature [12]:

$$D_{\mathrm{mol}}(T) = \frac{k_B T}{2\pi\mu R_d}\frac{\mu+\nu}{2\mu+3\nu}, \tag{10}$$

where $\mu$ is the dynamic viscosity of the solvent, and $R_d$ is the effective radius of the solute molecules with the "coefficient of sliding friction" $\beta$, $\nu = R_d\beta/3$. The dependence of dynamic viscosity on temperature can be described by a modified Frenkel formula [16]:

$$\mu(T) = \mu_0 \exp\frac{a}{T+\tau}. \tag{11}$$

For water, the coefficient $\mu_0 = 2.42 \times 10^{-5}$ Pa · s, $a = W/k_B = 570$ K ($W$ is the activation energy), and $\tau = -140$ K. For the effective diffusion coefficient $D$ we assume the same relative variation with temperature as for $D_{\mathrm{mol}}$.

### B. Numerical results

Numerical simulation was performed for an atmosphere composed solely of nitrogen: the single-component atmosphere approximation. Technical details on the numerical simulation are provided in the Appendix. The simulation reveals that for any initial condition, after a transient process, the system reaches a single stable time-periodic regime. Let us consider this regime.

The linear growth of the solubility with depth owned by the hydrostatic pressure gradient is modulated by the temperature wave, (3). The oscillating solubility profile, (1), for the temperature wave, (3), and pressure, (4), is shown in Fig. 1. Oscillations of the solubility profile lead to the formation of a profile of the net amount of gas molecules $X_\Sigma(z)$ that is nearly constant in time. The profile of the net molar fraction $X_\Sigma(z)$ nearly attains the maximal (midwinter) solubility next to the surface, $z = 0$; there the bubbly fraction exists for nearly the entire year except for the short coldest period. Further, $X_\Sigma(z)$ monotonically decreases with depth, along with the decrease in the time interval when the bubbly phase is present, down to the depth where the bubbly phase never appears. Below the latter depth $X_\Sigma(z) = X_s(z)$ is nearly uniform and only slightly changes during the year. Nonuniformity of the profile $X_\Sigma(z)$ in this zone rapidly decays with depth. The asymptotic value $X_\infty$ is close to the annual-mean surface solubility of the gas. These features of the regime are clearly shown in Figs. 2 and 3.

The net molar fraction profile is nearly constant during the year because the molecular diffusivity $D$ is 3 orders of magnitude lower than the heat diffusivity $\chi$, meaning that the diffusive redistribution of mass is a slow process against the background of a rapid temperature (and, hence, solubility) oscillation. This well-pronounced separation of time scales provides the opportunity to develop an analytical theory of the process, allowing for better insight into the mechanisms of the formation of the bubbly horizon. The results of numerical simulation also can be more comprehensively understood in the context of this theory.

### C. Analytical theory

The principal assumption of our analytical theory is that the net molar fraction profile $X_\Sigma$ is "frozen" for one oscillation period and the period-mean diffusion flux performs a slow diffusive transfer of the solute mass. For the analytical treatment we also linearize temperature dependencies of the diffusion coefficient,

$$D \approx D_0(1 + \delta_1 e^{-kz}\cos(\omega t - kz)), \tag{12}$$

and the solubility,

$$X^{(0)} \approx X_0^{(0)}(1+bz)(1 - a_1 e^{-kz}\cos(\omega t - kz)), \tag{13}$$

where $a_1 = -(\partial \ln X^{(0)}/\partial T)_P\,\Theta_0$, $\delta_1 = (\partial \ln D/\partial T)_P\,\Theta_0$, $b = \rho g/P_0$.

Prior to constructing the analytical theory, let us emphasize that this analytical theory is an approximation but not a limiting case. The linearizations (12) and (13) require a small $\Theta_0$. Meanwhile, for small $\Theta_0$ the penetration depth of the bubbly zone is small (below it is shown to be a nearly linear function of $\Theta_0$) and can become commensurable with the thickness of the diffusion boundary layer $\delta_{\mathrm{diff}} = \sqrt{2D/\omega}$. In the latter case the approximation of the frozen profile $X_\Sigma(z)$ is invalid. Thus, the frozen profile approximation is not compatible with the limit of vanishing $\Theta_0$. Nonetheless, for moderate $\Theta_0$, both approximations are satisfactory accurate.

For analytical calculations we take into account the order of magnitude of the relevant system parameters—$a_1|_{\Theta_0=15\,\mathrm{K}} \approx 0.2$, $\delta_1 \sim a_1$, $b = 0.1$ m$^{-1}$, and $k \approx 0.8$ m$^{-1}$—for the annual temperature oscillation in wetlands.

At a steady regime the annual-mean diffusive flux $\langle J\rangle$ is 0. For the porous-medium domain where the bubbly phase appears for some part of the oscillation period, the mean flux reads

$$\langle J\rangle = \frac{1}{t_p}\int_{t_1}^{t_2}\left(-D\frac{dX^{(0)}}{dz}\right)dt + \frac{1}{t_p}\int_{t_2}^{t_1+t_p}\left(-D\frac{dX_\Sigma}{dz}\right)dt, \tag{14}$$

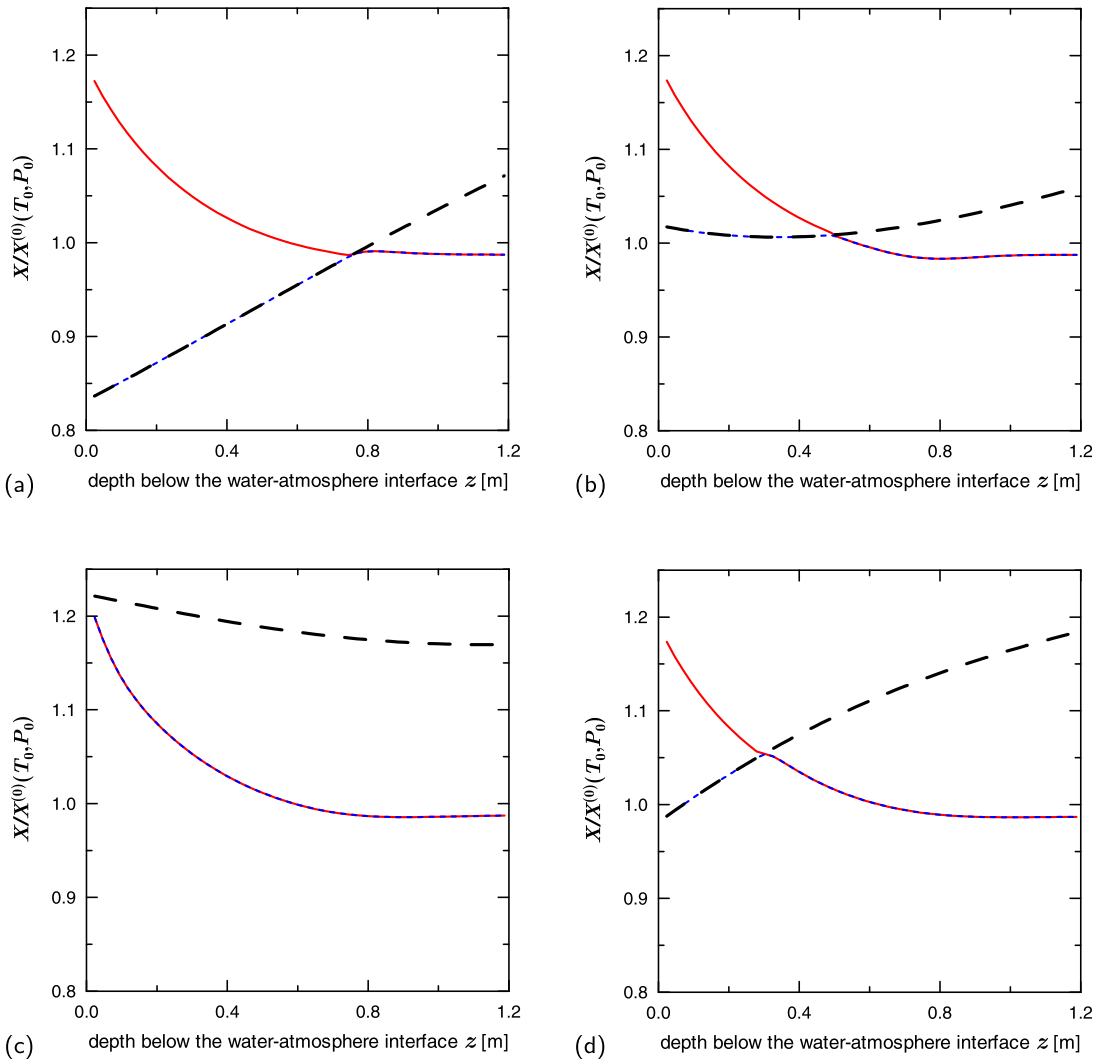


FIG. 1. (Color online) Snapshots of the oscillating solubility profile $X^{(0)}$ of nitrogen for the annual temperature wave in water-saturated ground (wetland) are plotted by dashed black lines for different surface temperature oscillation phases: (a) midwinter, (b) midspring, (c) midsummer, (d) and midautumn. For simplicity, the atmosphere is assumed to be pure nitrogen, the molar fraction of which, in the Earth's atmosphere, is 78.09%. Dotted (blue) lines represent the solution molar concentration $X_s$. Solid (red) lines show the net molar fraction $X_\Sigma$ of nitrogen molecules in the pore fluid. The bubbly fraction $X_b$ is given by the difference between the solid (red) and the dotted (blue) profiles (it does not exist for the cold winter period, when solubility is high). The net molar fraction is nearly unchanging during the year.

where $t_p = 2\pi/\omega$ is the oscillation period, and $t_1 < t_2$ are the instants in time between which the local temperature is high enough so that the local solubility becomes lower than $X_\Sigma$. Equation (14) can be rewritten in terms of the temperature oscillation phase $\varphi = \omega t - kz$:

$$\langle J\rangle = \frac{1}{2\pi}\int_{-\varphi_*}^{\varphi_*}\left(-D\frac{dX^{(0)}}{dz}\right)d\varphi + \frac{1}{2\pi}\int_{\varphi_*}^{\varphi_*+2\pi}\left(-D\frac{dX_\Sigma}{dz}\right)d\varphi, \qquad (15)$$

with $\varphi_* \in (0,\pi)$ determined by the condition $X^{(0)}(\varphi=\varphi_*) = X_\Sigma$; i.e.,

$$1 - a_1 e^{-kz}\cos\varphi_* = \frac{1}{1+bz}\frac{X_\Sigma}{X_0^{(0)}}. \qquad (16)$$

After laborious but straightforward mathematical manipulations, to the leading order, the equation $\langle J\rangle = 0$ with substitutions (12), (13), (15), and (16) takes the form

$$b\,\varphi_* + a_1(-b+k+\delta_1 b)e^{-kz}\sin\varphi_* + a_1 k\delta_1\left(\varphi_* - \frac{1}{2}\sin 2\varphi_*\right) + (\pi - \varphi_* - a_1\delta_1 e^{-kz}\sin\varphi_*) \times \left(b - \frac{d}{dz}(a_1 e^{-kz}\cos\varphi_*)\right) = 0. \qquad (17)$$

The latter equation should be treated as an initial value problem; it should be integrated from $\varphi_*(z=0)=\pi$ till $\varphi_*(z)$ attains 0, the point $z_b$ where $\varphi_* = 0$ is the base of the bubbly zone. For $z > z_b$, the bubbly phase never appears and $X_\Sigma$ is constant. It is more convenient to deal with Eq. (17) in terms

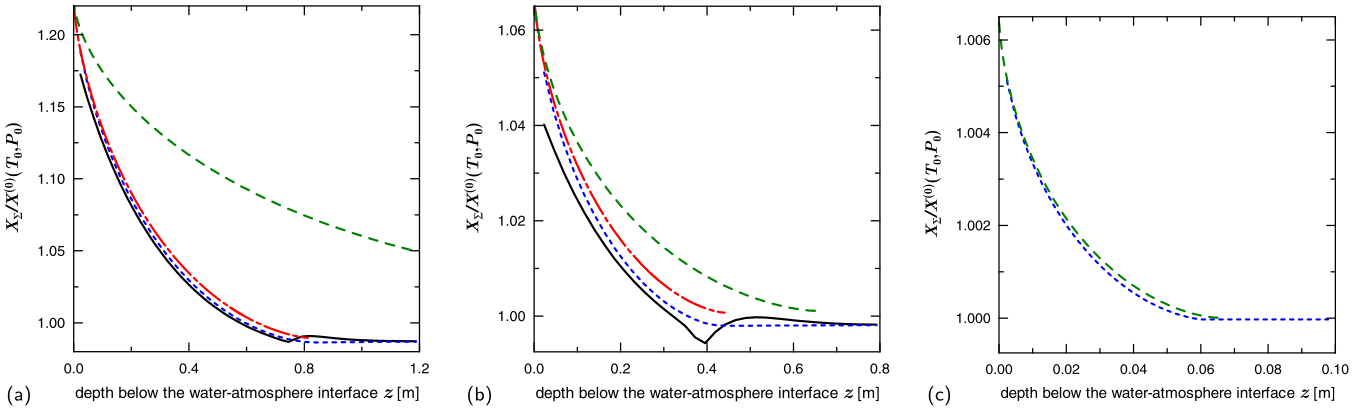


FIG. 2. (Color online) Profiles of the net molar fraction $X_\Sigma$ are plotted for temperature oscillation amplitudes $\Theta_0 = 15$ K (a), $\Theta_0 = 5$ K (b), and $\Theta_0 = 0.5$ K (c). Solid black lines represent the results of numerical simulation for the real molecular diffusion coefficient of nitrogen in water; dotted (blue) lines represent the results of numerical simulation with diminished values of the diffusion coefficient: $D = 0.01 D_{\mathrm{N_2,H_2O}}$ (a, b) and $D = 10^{-4} D_{\mathrm{N_2,H_2O}}$ (c). Dash-dotted (red) lines represent the analytical solution, (18); dashed (green) lines represent the limiting-case analytical solution, (20).

of $\xi = (b/a_1)z$, $\varkappa\xi = kz$, and $F = e^{-kz}\cos\varphi_*$:

$$\frac{d\xi}{dF} = \frac{\pi - \arccos(Fe^{\varkappa\xi})}{\pi + \varkappa\delta_1 e^{-2\varkappa\xi}\arccos(Fe^{\varkappa\xi})} \times \frac{-a_1\delta_1\sqrt{e^{-2\varkappa\xi} - F^2}}{+\left(\frac{a_1(k-b)}{b} - \frac{\varkappa\delta_1}{4}F\right)\sqrt{e^{-2\varkappa\xi} - F^2}}. \quad (18)$$

The latter equation should be integrated from $F = -1, \xi = 0$, which corresponds to the surface, till the equality $F = e^{-\varkappa\xi}$ is fulfilled, which corresponds to the base of the bubbly zone. In Figs. 2(a) and 2(b) the result of integration of Eq. (18) is plotted by the dash-dotted (red) lines. One can see that the analytical theory is in good agreement with the results of numerical simulation.

Equation (17) can be simplified for the limiting case $a_1 \to 0$ (where the depth of penetration of the bubbly zone is also small, meaning that $kz \to 0$):

$$\varphi_* + (\pi - \varphi_*)\left(1 + \sin\varphi_*\frac{d\varphi_*}{d\xi}\right) = 0. \quad (19)$$

The latter equation can be integrated and yields

$$(\pi - \varphi_*)\cos\varphi_* + \sin\varphi_* = \pi\xi. \quad (20)$$

For solution (20), the coordinate $\xi$ varies from 0 (surface) to $\xi_b = 1$ (the base of the bubbly zone). The net molar fraction profile is given by $X_\Sigma/X_0^{(0)} = 1 + a_1\xi - a_1\cos\varphi_*$. For this limiting solution, one can determine the scaling properties of the solution next to the surface for $\xi \ll 1$:

$$\frac{X_\Sigma}{X_0^{(0)}} = 1 + a_1 - \frac{a_1}{2}\left(\frac{3}{2}\pi\right)^{\frac{2}{3}}\xi^{\frac{2}{3}} + \cdots.$$

This limiting solution is plotted in Fig. 2 by the dashed (green) lines. Unfortunately, this limiting solution is accurate only for low amplitudes of temperature oscillations, where the diffusive

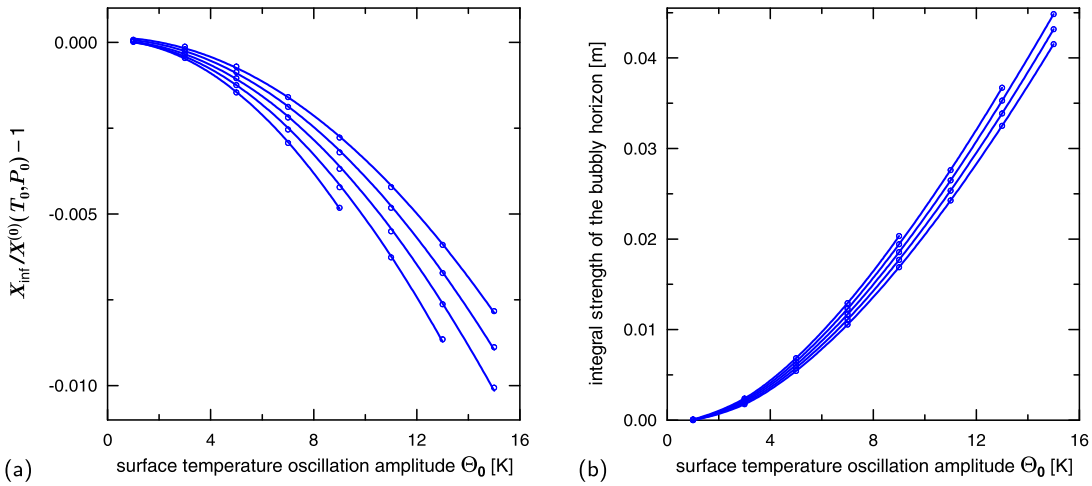


FIG. 3. (Color online) For a nitrogen atmosphere and water-saturated porous medium the bubbly-horizon quantifiers are plotted vs the surface temperature oscillation amplitude $\Theta_0$ for annual-mean temperatures $T_0 = 9$, 13, 17, 21, and 25 K [from bottom to top in (a) and from top to bottom in (b)]. (a) Lines are a quadratic fitting of the calculated data plotted by symbols.

boundary layer $\xi_{\rm diff} = (b/a_1)(2D/\omega)^{1/2}$ is commensurable with the bubbly-zone thickness $\xi_b = 1$ and thus the assumption of the frozen profile is not valid for typical diffusivities in liquids.

In order to ensure the correctness of analytical calculations, numerical simulation was performed for a diminished molecular diffusion $D$. The molecular diffusion coefficient was small enough for both assumptions of the analytical theory to be simultaneously accurate. In Figs. 2(a) and 2(b), one can see that the results of analytical theory, (18), match the results of numerical simulation for a 100-fold diminished $D$ plotted by dotted (blue) lines. In Fig. 2(c), the limiting analytical solution, (20), matches the numerical results for the diffusion coefficient diminished by a factor of $10^4$. Considering the results of numerical simulation for diminished diffusivity, one can note the disappearance of the kink near the boundary between the bubbly horizon and the zone of undersaturated solution, which is shown in Figs. 1, 2(a), and 2(b) for a "normal" diffusion strength. Thus, one can conclude that this kink is related to the finiteness of the ratio $D/\chi$. The $X_\Sigma$ profile is not completely frozen on the time scale of temperature oscillations; at the point of discontinuity of the solute concentration gradient even a low diffusivity can result in an observable distortion of the net profile $X_\Sigma$.

The case of impaired diffusion can also be of physical interest for porous media where the pore network is not globally connected and diffusive transport necessarily involves diffusion through the solid matrix material separating different connected clusters of pores from each other. In this case the effective diffusion coefficient will be diminished by several orders of magnitude compared to the bulk diffusivity in the pore liquid.

### D. Integral quantifiers of the bubbly horizon

The developed analytical theory suggests natural quantifiers of the $X_\Sigma$ profile: the deep solute concentration $X_\infty/X_0^{(0)}$ and the integral strength of the bubbly layer $I = \langle\int[(X_\Sigma - X_\infty)/X_0^{(0)}]dz\rangle$. These characteristics are good quantifiers of the system state even for situations where the $X_\Sigma$ profile is far from being frozen (see Fig. 2). In Fig. 3, the quantifiers $X_\infty$ and $I$ are plotted for a nitrogen atmosphere and water-saturated porous medium. The deviation of $X_\infty$ from the annual-mean near-surface solubility is a nonlinear effect, quadratic in amplitude $\Theta_0$. For nonvanishing $\Theta_0$ the effect is negative; i.e., the temperature oscillation results in "ventilation" of deep areas of the porous medium.

## III. THE CASE OF NO EFFECT OF THE PRESSURE GRADIENT

For the annual temperature wave the penetration depth $1/k = \sqrt{2\chi/\omega}$ is about 1 m; for this depth the hydrostatic pressure increase is comparable to the atmospheric pressure, and thus, the gas solubility is significantly influenced by the hydrostatic pressure gradient. For higher oscillation frequencies in nature (e.g., daily oscillations) and technological systems

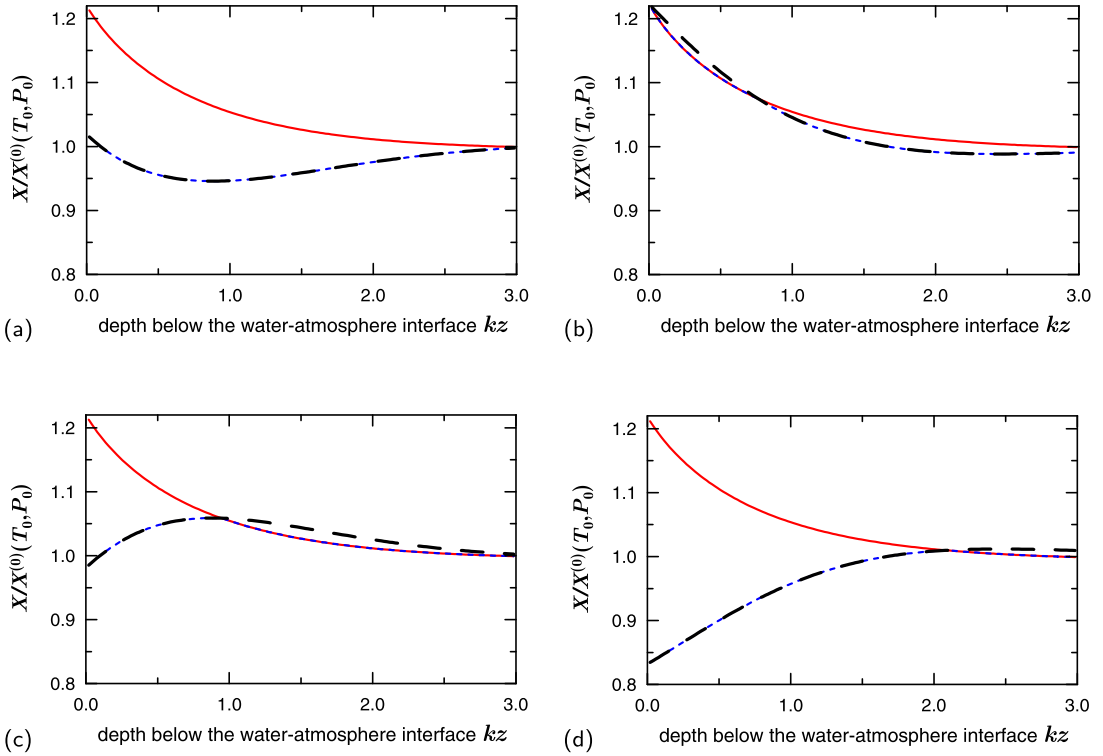


FIG. 4. (Color online) Dynamics of the bubbly horizon in porous medium in the absence of a hydrostatic pressure gradient is presented for a nitrogen atmosphere. Snapshots of profiles of $X^{(0)}(z)$ [dashed (black) lines], $X_s(z)$ [dotted (blue) lines], and $X_\Sigma(z)$ [solid (red) lines] are plotted for different phases $\varphi$ of the surface temperature oscillation: (a) $\varphi(z=0) = 0$, (b) $\varphi(z=0) = \pi/2$, (c) $\varphi(z=0) = \pi$, and (d) $\varphi(z=0) = 3\pi/2$. Results are provided in dimensionless form and are valid for arbitrary oscillation frequency.

the hydrostatic pressure increase for the wave penetration depth can be negligible. The case of solutions of solids and liquids is qualitatively similar to the case of no hydrostatic pressure gradient, as the solubility of condensed matter is nearly independent of the pressure [see Eq. (2)].

In Fig. 4, one can see that in the absence of a pressure gradient the bubbly horizon is not bounded from below. For any depth $z$ the solubility profile $X^{(0)}$ exceeds the $X_\Sigma$ profile (i.e., the bubbly phase locally disappears) for a small fraction of the oscillation period; $X_\Sigma(z)$ is slightly smaller than the envelope of the wave of $X^{(0)}(z,t)$. For the limit of vanishingly low ratio $D/\chi$ the $X_\Sigma$ profile coincides with the envelope of $X^{(0)}(z,t)$. While the envelopes of solubility profiles are different for gaseous and condensed matter, the principle, that the $X_\Sigma(z)$ profile tends to coincide with the envelope of the solubility profile wave, remains valid for solids and liquids. Hence, the integral strength of the bubbly horizon is approximately

$$I = \int_0^{+\infty} a_1 e^{-kz} dz = \left| \frac{\partial \ln X^{(0)}}{\partial T} \right|_P \frac{\Theta_0}{k}. \qquad (21)$$

## IV. CONCLUSION

We have considered the diffusion transport of a weakly soluble substance in a liquid-saturated porous medium half-space in contact with a reservoir of this substance in the case where the surface temperature harmonically oscillates in time. The surface temperature oscillation creates a temperature wave which propagates deep into the porous medium and decays with depth. The solubility wave associated with the temperature wave results in time-dependent intermittency of the zones of nondissolved phase with saturated solution and the zones of undersaturated solution.

Due to the low value of the ratio $D/\chi$, which is as low as $\sim 10^{-3}$ for transport processes in liquids, the diffusion transport in the system is much slower than the temperature (and solubility) variation. As a result, the profile of the net molar fraction of "guest" molecules in pores, $X_\Sigma$ ("net" means "solute + nondissolved phase"), remains nearly constant over the oscillation period. We have revealed *for gases* that the $X_\Sigma$ profile nearly attains the maximal-per-period solubility next to the surface; monotonously decays with depth in the zone where the nondissolved phase can be observed, the bubbly horizon; and reaches a constant level beneath the bubbly horizon (Fig. 2). The bottom boundary of the bubbly horizon is controlled by the hydrostatic pressure gradient.

Without the pressure gradient, the bubbly horizon is not bounded from below and the $X_\Sigma$ profile is slightly smaller than the envelope of the oscillating solubility profile (Fig. 4). At any depth $z$ the bubbly phase disappears for only a short portion of the oscillation period; in the idealistic limiting case $D/\chi \to 0$ this part of the oscillation period tends to 0. Note that the solubility profile decays with the depth exponentially, and thus, even though the bubbly horizon is not formally bounded from below, the volumetric fraction of bubbles in pores exponentially tends to zero at the depth, meaning the bubbly horizon to nearly disappear there. The no-pressure-gradient case is relevant for gases and short-term oscillations, when the penetration depth of the temperature wave is small compared to the depth scale of a noticeable increase in the hydrostatic pressure, and for condensed phases, the solubility of which is insensitive to pressure.

For the reported results an analytical theory, which lends better insight into the mechanisms of the phenomenon, has been developed [Eqs. (18) and (20)].

For an annual temperature oscillation of amplitude 15 K the atmosphere gas bubbly horizon has been found to have an 0.8-m penetration depth and a near-surface relative increase in $X_\Sigma$ of 20% compared to the no-oscillation solubility [Fig. 2(a)]. Such an effect can be considered non-negligible for the local conditions for microflora and fauna. The dependence of integral quantifiers of the bubbly horizon on the average surface temperature and temperature oscillation amplitude is plotted in Fig. 3.

The periods of negative temperatures with frozen groundwater are beyond the scope of this study and will be considered elsewhere.

## ACKNOWLEDGMENTS

The authors acknowledge financial support from the Government of Perm Region (Contract C-26/0004.3) and the Russian Foundation for Basic Research (Project No. 14-01-31380_mol_a).

## APPENDIX: NUMERICAL SIMULATION

The evolution of Eq. (7) was simulated with a finite-difference method, an explicit scheme with central differences. The time-dependent fields of temperature, molecular diffusion coefficient, and solubility were precalculated for one cycle of the surface temperature oscillation on the space-time grid used for simulation of Eq. (7). The calculation domain was limited from below by the depth $L_\infty$, and boundary condition (9) was moved to $z = L_\infty$; the depth $L_\infty$ was chosen so that perturbations of the solute concentration profile were not visually resolvable at $z = L_\infty/2$. The choice of the space step size was guided by two requirements. First, a decrease in the step size by half should not change the results of simulation by more than 1%. Second, for a diffusion coefficient diminished by a factor of $10^{-4}$ the relative mismatch between the results of numerical simulation and the unsimplified analytical solution, (17), should not exceed 0.1%. Practically, grids with 30–50 points per the zone of nondissolved phase were sufficiently detailed for these requirements to be met. The time step size was determined by the requirement of stability of the explicit method.

[1] J. H. Donaldson, J. D. Istok, M. D. Humphrey, K. T. O'Reilly *et al.*, Development and testing of a kinetic model for oxygen transport in porous media in the presence of trapped gas, Ground Water **35**, 270 (1997); J. H. Donaldson, J. D. Istok, and K. T. O'Reilly, Dissolved gas transport in the presence of a trapped gas phase: Experimental evaluation of a two-dimensional kinetic model, *ibid.* **36**, 133 (1998).

[2] R. R. Haacke, G. K. Westbrook, and M. S. Riley, Controls on the formation and stability of gas hydrate-related bottom-simulating reflectors (BSRs): A case study from the west Svalbard continental slope, J. Geophys. Res. **113**, B05104 (2008).

[3] D. S. Goldobin and N. V. Brilliantov, Diffusive counter dispersion of mass in bubbly media, Phys. Rev. E **84**, 056328 (2011).

[4] P. V. Krauzin and D. S. Goldobin, Effect of temperature wave on diffusive transport of weakly soluble substances in liquid-saturated porous media, Eur. Phys. J. Plus **129**, 221 (2014).

[5] M. K. Davie and B. A. Buffett, A numerical model for the formation of gas hydrate below the seafloor, J. Geophys. Res. B **106**, 497 (2001).

[6] D. S. Goldobin, Non-Fickian diffusion affects the relation between the salinity and hydrate capacity profiles in marine sediments, C.R. Mecan. **341**, 386 (2013).

[7] D. S. Goldobin, N. V. Brilliantov, J. Levesley, M. A. Lovell *et al.*, Non-Fickian diffusion and the accumulation of methane bubbles in deep-water sediments, Eur. Phys. J. E **37**, 45 (2014).

[8] J. R. Petit, J. Jouzel, D. Raynaud, N. I. Barkov *et al.*, Climate and atmospheric history of the past 420000 years from the Vostok ice core, Antarctica, Nature **399**, 429 (1999); EPICA Community Members, Eight glacial cycles from an Antarctic ice core, *ibid.* **429**, 623 (2004).

[9] S. J. Hunter, D. S. Goldobin, A. M. Haywood, A. Ridgwell, and J. G. Rees, Sensitivity of the global submarine hydrate inventory to scenarios of future climate change, Earth Planet. Sci. Lett. **367**, 105 (2013).

[10] R. A. Pierotti, A scaled particle theory of aqueous and nonaqueous solutions, Chem. Rev. **76**, 717 (1976).

[11] E. D. Yershov, *General Geocryology* (Cambridge University Press, New York, 1998).

[12] R. B. Bird, W. E. Stewart, and E. N. Lightfoot, *Transport Phenomena* (Wiley, New York, 2007).

[13] S. J. Gregg and K. S. W. Sing, *Adsorption, Surface Area and Porosity* (Academic Press, New York, 1982).

[14] B. A. Buffett and O. Y. Zatsepina, Formation of gas hydrate from dissolved gas in natural porous media, Mar. Geol. **164**, 69 (2000).

[15] R. Anderson, B. Tohidi, and J. B. W. Webber, Gas hydrate growth and dissociation in narrow pore networks: Capillary inhibition and hysteresis phenomena, in *Sediment-Hosted Gas Hydrates: New Insights on Natural and Synthetic Systems. Geological Society London Special Publications 319*, edited by D. Long, M. A. Lovell, J. G. Rees, and C. A. Rochelle (Geological Society London, London, 2009), p. 145.

[16] J. Frenkel, *Kinetic Theory of Liquids* (Dover, Mineola, NY, 1955).

[17] V. I. Baranenko, V. S. Sysoev, L. N. Fal'kovskii, V. S. Kirov *et al.*, The solubility of nitrogen in water, At. Energy **68**, 162 (1990); V. I. Baranenko, L. N. Fal'kovskii, V. S. Kirov, L. N. Kurnyk *et al.*, Solubility of oxygen and carbon dioxide in water, *ibid.* **68**, 342 (1990); S. Yamamoto, J. B. Alcauskas, and T. E. Crozier, Solubility of methane in distilled water and seawater, J. Chem. Eng. Data **21**, 78 (1976).

[18] P. T. H. M. Verhallen, L. J. P. Oomen, A. J. J. M. v. d. Elsen, A. J. Kruger, and J. M. H. Fortuin, The diffusion coefficients of helium, hydrogen, oxygen and nitrogen in water determined from the permeability of a stagnant liquid layer in the quasi-steady state, Chem. Eng. Sci. **39**, 1535 (1984); W. Sachs, The diffusional transport of methane in liquid water: Method and result of experimental investigation at elevated pressure, J. Petrol. Sci. Eng. **21**, 153 (1998); R. E. Zeebe, On the molecular diffusion coefficients of dissolved $CO_2$, $HCO_3^-$, and $CO_3^{2-}$ and their dependence on isotopic mass, Geochim. Cosmochim. Acta **75**, 2483 (2011).